



# Forecast climate change impact on porewater pressure regimes for the design and assessment of clay earthworks

Wengui Huang<sup>1</sup>, Fleur A. Loveridge<sup>2\*</sup>, Kevin M. Briggs<sup>3</sup>, Joel A. Smethurst<sup>4</sup>, Nader Saffari<sup>5</sup> and Fiona Thomson<sup>6</sup>

<sup>1</sup> School of Computing, Engineering & Digital Technologies, Teesside University, Middlesbrough TS1 3BX, UK

<sup>2</sup> School of Civil Engineering, University of Leeds, Leeds LS2 9JT, UK

<sup>3</sup> Department of Architecture and Civil Engineering, University of Bath, Bath BA2 7AY, UK

<sup>4</sup> School of Engineering, University of Southampton, Southampton SO17 1BJ, UK

<sup>5</sup> Engineering (Earth Structures & Geotechnical), Transport for London, London E20 1JN, UK

<sup>6</sup> Engineering & Asset Strategy, Transport for London, London E20 1JN, UK

WH, 0000-0002-4177-8156; FAL, 0000-0002-6688-6305; KMB, 0000-0003-1738-9692

\* Correspondence: [F.A.Loveridge@leeds.ac.uk](mailto:F.A.Loveridge@leeds.ac.uk)

**Abstract:** Understanding and mitigating the impact of climate change on the built environment is becoming increasingly important worldwide. Earthworks (embankments and cuttings) supporting road and rail transportation networks often have direct contact with the atmosphere and are therefore influenced by extreme weather events and seasonal weather patterns. Atmospheric wetting and drying alters porewater pressures (PWP) within earthworks, potentially contributing to the deformation and failure of earthwork slopes. Consequently, it is essential to understand the influence of climate change on PWP within earthwork slopes, to inform strategies for their design, assessment and maintenance. Extensive 1D seepage analyses were carried out for typical railway embankments in the London area. The analyses showed that forecast hotter, drier summers will increase the water storage capacity of earthworks. This will lead to increased net infiltration in the winter months owing to both a forecast increase in rainfall and a longer time being required to saturate the soil pores and bring the water table back to the slope surface. Hence, despite the forecast increase in winter rainfall, this will not lead to higher design PWP regimes. The analyses were conducted for the London area, but this approach and conceptual framework can be readily adapted for other locations.

**Thematic collection:** This article is part of the Climate change and resilience in Engineering Geology and Hydrogeology collection available at: <https://www.lyellcollection.org/topic/collections/Climate-change-and-resilience-in-engineering-geology-and-hydrogeology>

Received 24 February 2023; revised 28 July 2023; accepted 25 September 2023

Understanding and mitigating the impact of climate change is becoming an increasing challenge worldwide. All infrastructure can be affected by climate change; for example, predicted increases in the frequency of extreme temperatures and severe flooding will lead to damage to transport networks (CCC 2021; Dodman *et al.* 2022). Geotechnical structures are specifically vulnerable to climate effects as they often have direct contact with the atmosphere (Tarantino *et al.* 2016). Climate change effects could be coupled with increasing human disturbance and activities, which further drives risk (Zhang *et al.* 2013, 2022; Ozturk *et al.* 2022). The UK independent assessment of climate risk rates the potential adverse impacts from slope and embankment failure on transport networks as its highest urgency score (CCC 2021). This risk is compounded by the age (up to 170 years) of many transport embankments and cuttings in the UK (Spink 2020), which are known to be deteriorating (e.g. Briggs *et al.* 2017; Rouainia *et al.* 2020; Postill *et al.* 2021). For example, data from Network Rail show annual failure rates of 0.06% and 0.27% for soil embankments and cuttings respectively between April 2019 and March 2020. These annual rates are respectively three and two times the average rates recorded for the 17 years from 2003 to 2020 (Mair 2021).

In the UK, there is no discernible trend in annual precipitation but a clear trend for annual temperature, in both the historical weather record (Lee 2020) and future climate projections (Jenkins *et al.* 2009; Lowe *et al.* 2018a). The increase in temperature is projected

to have an impact on seasonality, with summer becoming hotter and drier, and winter warmer and wetter (Dixon and Brook 2007; Jenkins *et al.* 2009; Lowe *et al.* 2018b). These changes are expected to lead to adverse impacts for both natural slopes (e.g. Moore *et al.* 2010) and earthworks (e.g. Rouainia *et al.* 2020). One way in which climate change will influence earthwork behaviour is by altering porewater pressure (PWP) regimes within earthwork slopes. PWP directly affect the effective stresses governing soil strength and volume change. This influences the stability (ultimate limit state) and deformation (serviceability limit state) of earthworks. PWP are influenced by the infiltration and removal of water at or near the slope surface owing to rainfall and evapotranspiration respectively (e.g. Zhang *et al.* 2004; Smethurst *et al.* 2006, 2012; Lee *et al.* 2009; Briggs *et al.* 2013a, 2016). Climate change could alter the magnitude, duration and timing of rainfall infiltration and evapotranspiration. Consequently, it is essential to understand the effect of these changes on PWP development. If climate change causes higher PWP, it would mean that many existing slopes that were designed using PWP guidelines based on the past climate may not be safe in the future climate. Furthermore, PWP guidelines (e.g. LUL 2019) would need to be updated to take into account the effect of climate change for the design of new slopes and the adaptation and remediation of existing slopes. Alternatively, if greater climate-induced drying reduces future PWP then there is the potential for a less conservative approach in the future.

The aim of this study is to investigate the effect of forecast climate change on porewater pressure regimes within transport infrastructure earthworks in the SE England. This study first reviews recent approaches to the assessment of climate impacts on geotechnical structures. Appropriate and up-to-date climate data are then selected and prepared using the UK Climate Projections 2018 (UKCP18) future scenarios. To allow a full consideration of climate uncertainty and investigate the effects of soil permeability and vegetation types, an efficient modelling strategy is adopted, and this is explained. The key indicators used to interpret the simulations are introduced, and the results showing the impact of climate change on future water balance and PWP are given.

## Climate impacts assessment approach

Coe and Godt (2012) summarized research on the effect of climate change on geotechnical structures into three categories: monitoring approach, retrospective approach and prospective approach. The monitoring approach requires long-term monitoring, which is essential but can be time-consuming and costly. Both the monitoring and retrospective approaches implicitly assume that the observations in the past can be extrapolated to the future, which may not be valid in the context of climate change (Dijkstra and Dixon 2010; Tang *et al.* 2018). There is increasing capability in forecasting of future climate and the numerical modelling of geotechnical structures, making it an attractive approach that complements long-term monitoring. Table 1 provides an extensive (but not exhaustive) summary of work using this approach. Research has been carried out to investigate the effects of climate change on various geotechnical structures including natural slopes, transport embankments and cuttings at various locations. It should be noted that climate data are site specific, and therefore conclusions for a particular site and geological context may not necessarily be generalized to other locations (Vardon 2015; Gariano and Guzzetti 2016; Tang *et al.* 2018; Fowler *et al.* 2021). In addition, the ability to forecast future climate has improved in recent decades. A good example is the climate projections for the UK, which have developed from CCIRG91 (1991), through UK Climate Impacts Programme 2002 (UKCIP02; Hulme *et al.* 2002) and UK Climate Projections 2009 (UKCP09; Jones *et al.* 2009) to the current UKCP18 (Murphy *et al.* 2018), underpinned by improved climate models of higher resolution. However, there are still various uncertainties associated with future climate modelling (Palin *et al.* 2021): (1) uncertainty in the future carbon emission scenarios; (2) modelling uncertainty, arising from our incomplete knowledge, which limits our ability to model the climate system; (3) natural climate variability; (4) aleatory (irreducible) uncertainty, arising from intrinsic statistical variations of the system being modelled. The uncertainties are often captured through multiple climate models for future projections, as shown in Table 1.

Most of the existing studies shown in Table 1 used 2D coupled seepage–stability analysis. This approach is widely viewed as the gold standard for analyses of individual sites involving unsaturated geomaterials and a climate boundary. However, it is computationally expensive in this context, where many scenarios must be considered to account for uncertainty or the long time periods over which computation is required to capture decades of predicted changes. Therefore, simplifications are often made; for example, by investigating only extreme rainfall events (Robinson *et al.* 2017; Vahedifard *et al.* 2017) or considering only a limited number of climate models over relatively short time periods (Rouainia *et al.* 2020; Guo 2021). However, Lieber *et al.* (2022) highlighted that using projected climate for a snapshot of time could lead to overconservative design. Instead, using long-term climate data (both historical and projected) could give a more reasonable design solution. Another simplification is not to test the effects of soil

permeability and vegetation types (Guo 2021; Pk *et al.* 2021), but this misses important controls on both infiltration and evapotranspiration, which ultimately affect PWPs.

In this study, because the research objective is to investigate the effect of climate change, it is argued that more comprehensive consideration should be given to the climate data at the cost of using a simple yet computationally efficient 1D soil model. Bussi re *et al.* (2007) showed that 1D seepage analysis can provide a good estimate of the hydrological response of the central part of a landfill cover system. Meanwhile, Briggs *et al.* (2013b) also demonstrated that a 1D seepage analysis closely approximates the mid-slope condition within a 2D analysis. A similar approach is also successfully adopted by Lieber *et al.* (2022) to investigate the effect of climate change on the performance of a tailings cover.

The details of the 1D hydrological model used in this study are described below in the section on finite-element seepage analysis. Because of the high computational efficiency of the 1D model, a wide breadth of scenarios of climate projections from UKCP18 (described in the next section) can be fully adopted in the finite-element seepage analysis. In addition, the effects of soil permeability and vegetation types are investigated through a series of parametric studies (described below) in the context of climate change.

## Climate data

### Introduction to UK climate projections 2018 (UKCP18)

The climate data used in this study were taken from UK climate projections 2018 (UKCP18), which is the latest national set of climate projections for the UK (Murphy *et al.* 2018). UKCP18 uses one of the latest versions of the Met Office United Model, HadGEM3-GC3.05 (hereafter GC3.05), and provides spatially coherent climate projections that can be conveniently used for site-specific analysis to develop narratives on the impact of climate change (Murphy *et al.* 2018). The projections were developed through a perturbed parameter ensemble (PPE) approach, which is a way to model climate uncertainties by perturbing model parameters within expert-specified ranges (Sexton *et al.* 2021; Yamazaki *et al.* 2021). Twelve PPEs from GC3.05 were selected by UKCP18 to downscale to regional (12 km) and local (2.2 km) scales. Both regional and local projections can better resolve physiographic features (e.g. mountains, urban effects, inland water bodies) relative to the global projections. The local projections can better simulate convective rainstorm events, and were therefore used in this study.

UKCP18 local projections provide rainfall data directly and also the climate variables required to determine potential evapotranspiration (PET). Bormann (2011) provided a comprehensive review of 18 models that can be used to estimate PET, and concluded that PET models should be validated in a regional context. Despite some debate (e.g. Chun *et al.* 2012), the Penman–Monteith method is one of the most commonly used models for calculating PET in the UK, and has been used for site-specific analyses (e.g. Postill *et al.* 2021; Yu *et al.* 2021) and to derive national sets of PET from climate observations 1969–2021 (Brown *et al.* 2022) and UKCP18 regional projections 1980–2080 (Robinson *et al.* 2021). Therefore, the Penman–Monteith method was also used in this study and PET was calculated as (Allen *et al.* 1998)

$$\text{PET} = \frac{0.408\Delta(R_n - G) + \gamma[900/(T + 273)]u_2(e_s - e_a)}{\Delta + \gamma(1 + 0.34u_2)} \quad (1)$$

where  $\Delta$  is the slope of the vapour pressure curve ( $\text{kPa } ^\circ\text{C}^{-1}$ ),  $R_n$  is the net solar radiation ( $\text{MJ m}^{-2} \text{day}^{-1}$ ),  $G$  is the surface heat flux ( $\text{MJ m}^{-2} \text{day}^{-1}$ ),  $\gamma$  is the psychrometric constant ( $\text{kPa } ^\circ\text{C}^{-1}$ ),  $T$  is the mean daily air temperature ( $^\circ\text{C}$ ),  $e_s$  and  $e_a$  are the saturation and

**Table 1.** Summary of numerical studies on effects of climate change on geostructures

References	Site location	Geostructure	Climate data		Modelling of climate change	Length of simulation	Modelling approach
			Historical (baseline)	Future (projected)			
Vahedifard <i>et al.</i> (2017)	Seattle, USA	Reinforced soil embankment wall	1950–1999	20 CMIP5 models for RCP8.5 and the period 2050–2099	1 day and 7 day extreme precipitations (95th upper percentile)	8 days for baseline, and 8 days for the projected. In total: 16 days	2D coupled seepage–stability analysis
Robinson <i>et al.</i> (2017)	Seattle, USA	Natural slope	1950–1999	20 CMIP5 models for RCP8.5 and the period 2050–2099	7 day extreme precipitation (95th upper percentile)	15 days for baseline, and 15 days for the projected. In total: 30 days	2D coupled seepage–stability analysis
Pk <i>et al.</i> (2021)	Toronto, Canada	Highway embankment	1981–2010	12 models of various sources for 2011–2100	(1) Long-term daily precipitation and evaporation (2 subset periods); (2) 1 h extreme precipitation	30 years for baseline, and 60 years for the projected. In total: 90 years	2D seepage–stability analysis
Lieber <i>et al.</i> (2022)	Quebec, Canada	Tailings cover	2015–2018	18 CMIP5 and CORDEX models for RCP4.5 and RCP8.5 and the period 2020–2100	(1) 2 month drought; (2) driest year; (3) 80 year. Out of 18 climate models, three were selected	4 years for baseline, and 243 years for the projected. In total: 247 years	1D seepage analysis (for both water and air flow)
Collison <i>et al.</i> (2000)	Kent, UK	Natural slope	1960–1990	Downscaled GCM (CCIRG91) for 1990–2079	Long-term daily precipitation and evapotranspiration	30 years for baseline, and 90 years for the projected. In total: 120 years	1D seepage–stability analysis
Dixon and Brook (2007)	Derbyshire, UK	Natural slope	1960–1990	UKCIP02 for medium-high scenario and 2080s	Long-term average of monthly precipitations	–	Statistical rainfall threshold analysis
Rouainia <i>et al.</i> (2009)	Newbury, UK	Railway embankment	UKCIP02 for 2003 scenario	UKCIP02 high emission for a 2080 scenario	Long-term daily precipitation and evapotranspiration	20 years for baseline, and 20 years for the projected. In total: 40 years	2D seepage–stability analysis
Clarke and Smethurst (2010)	London, Hemsby, Ringway, Yeovilton, UK	Engineered clay slopes	1961–2005 for London; 1961–1990 for the others	UKCIP02 for all emission scenarios from low to high, and for 2011–2100	Long-term daily precipitation and evapotranspiration	Baseline: 45 years for London, and 30 years for the other sites; projected: 90 years for each site. In total: 485 years	1D soil-water balance model
Booth (2014)	Newbury, UK	Highway cutting	UKCP09 control period (1961–1990)	UKCP09 weather generator for high emissions and 2040–2069	Long-term daily precipitation and evapotranspiration	100 model runs, and for each 1 year was selected for baseline and the projected. In total: 200 years	2D seepage analyses
Rouainia <i>et al.</i> (2020)	Newbury, UK	Highway cutting	UKCP09 control period (1961–1995)	UKCP09 weather generator for high emissions and 2000–2100	Long-term daily precipitation and evapotranspiration	100 years for the baseline, and 100 years for the projected. In total: 200 years	2D coupled seepage–stability analysis
Guo (2021)	Essex, UK	Railway and flood embankment	1971–2000, 2007–2020	UKCP18 regional projection (RCP 8.5) for the period 2021–2080	Long-term monthly precipitation and evapotranspiration	45 years for baseline, and 60 years for the projected. In total: 105 years	2D coupled seepage–stability analysis

CMIP, Coupled Model Intercomparison Project.

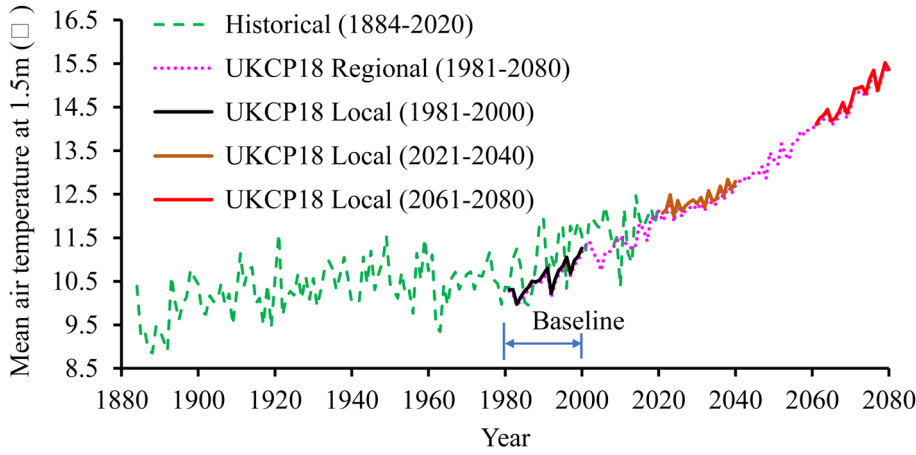


**Fig. 1.** Annual average mean air temperature at 1.5 m ( $^{\circ}\text{C}$ ) from the historical weather record (1884–2020) and UKCP18 projections (1981–2080, average of 12 PPEs) for Heathrow.

actual vapour pressure (kPa), respectively, and  $u_2$  is the wind speed at 2 m height ( $\text{m s}^{-1}$ ).

The climate variables from UKCP18 local projections are for three discontinuous periods 1981–2000, 2021–2040 and 2061–2080. It should be noted that the climate variables for the historical period (i.e. 1981–2000) are not the same as the historical weather record. However, they have been calibrated with historical weather records (Yamazaki *et al.* 2021) and therefore can be used as a baseline. There is uncertainty in future carbon emissions. UKCP18 local projections assume the highest carbon emissions scenario, RCP8.5, where RCP is representative contraction pathway (Meinshausen *et al.* 2011). For a given carbon emission scenario, there is still uncertainty in the future climate projections. The uncertainty is captured by the 12 diverse PPEs covering a broad range of climate scenarios (Murphy *et al.* 2018).

### Location of the site

Climate data are site specific. Initial sensitivity studies showed that much of the north and west of the UK was likely to retain hydrostatic worst-case PWP conditions, and therefore a location with greater drying was chosen to understand the nuance of future porewater pressure changes in a region subjected to greater change. This study therefore focuses on the London area, which is a region with significant drying potential (Harrison *et al.* 2012) and the highest density of infrastructure earthworks in the UK. The UKCP18 climate projections were taken for London Heathrow Airport. Figure 1 shows a comparison of annual average mean air temperature ( $T_{\text{mean}}$ ) at 1.5 m (above the ground surface) from the historical weather record and for clarity averages of the 12 individual PPEs from UKCP18 local and regional projections. It should be noted that averages of the 12 PPEs give a low variability, but a higher variability can be observed in the individual PPEs (Huang *et al.* 2023) and in the historical weather record. An increasing trend of  $T_{\text{mean}}$  can be observed from the historical records. The average  $T_{\text{mean}}$  was  $10.2^{\circ}\text{C}$  for 1901–1920 and  $11.7^{\circ}\text{C}$  for 2001–2020, and is projected to increase further to  $14.7^{\circ}\text{C}$  for 2061–2080 assuming carbon emissions follow RCP8.5. Figure 1 shows that UKCP18 local and regional projections give identical results for  $T_{\text{mean}}$ , but regional projections significantly over-predict annual rainfall compared with both local projections and historical records for this site (not shown). This was also a reason why this study adopted the UKCP18 local projections.

### Change of climate pattern

The annual rainfall and PET derived using equation (1) for the UKCP18 local projections are shown in Figure 2 as box plots. Each

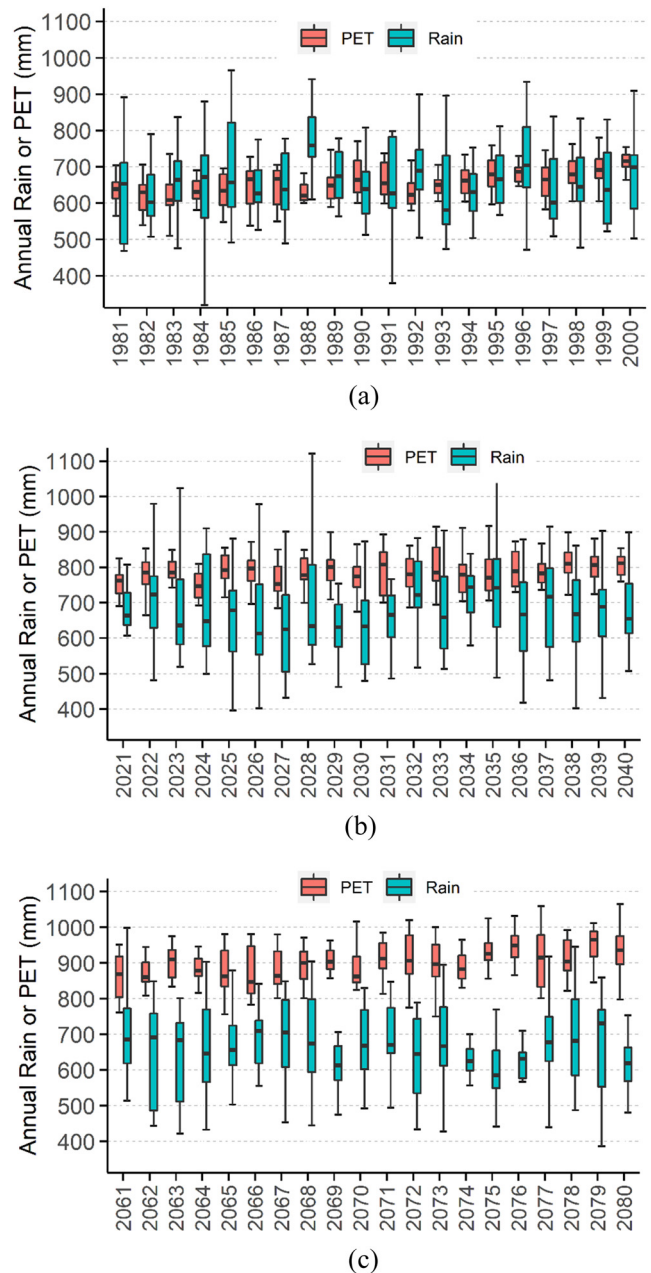


**Fig. 2.** Annual rainfall and potential evapotranspiration (PET) from UKCP18 local projections for London Heathrow. (a) 1981–2000; (b) 2021–2040; (c) 2061–2080.

box plot shows the minimum, 25th percentile, median, 75th percentile and maximum values of the projections. The magnitude of the annual rainfall and PET are comparable for 1981–2000. There is clearly an increase in PET with time, which is attributed to the increase in temperature shown in Figure 1. No clear trend is shown for annual rainfall with time, which is consistent with the observations in the historical weather record (Lee 2020) and climate projections (Jenkins *et al.* 2009; Lowe *et al.* 2018a). The annual PET is clearly above annual rainfall by 2061–2080 (Fig. 2c). Comparisons of monthly averages for rainfall and PET are shown in Figure 3. In summer, which is defined as from April to September in this study, there is an increase in PET and decrease in rainfall with time. In the winter months (October to March), there is a slight increase in PET with time, but significantly greater rainfall, particularly in mid-winter (December, January and February). The change of rainfall pattern (i.e. decrease in summer and increase in winter) can also be attributed to future changes in temperature. Atmospheric water-holding capacity is expected to increase exponentially with temperature (Min *et al.* 2011). The projected increase of temperature is greater in summer than in winter in southern England (Murphy *et al.* 2018). Consequently, more water is expected to be held in the atmosphere in summer, leading to reduced rainfall, whereas the water-holding capacity is reached in winter, leading to greater rainfall.

### Finite-element seepage analysis

The finite-element program SEEP/W, which is part of the GeoStudio software package, was adopted in this study. Therefore, only the hydrological response of a slope owing to climate change was considered. Although neglecting the mechanical response to pore-water pressure changes removes a direct link to stability assessment, the results can still be used to infer its effect on known mechanisms of earthwork deterioration, or as an input to non-coupled stability analysis. By ignoring water compressibility, vapour transfer and thermal effects, the governing equation for water flow in porous medium can be written as (Geo-Slope International 2020)

$$m_v \frac{\partial u_w}{\partial t} + m_w \frac{\partial(u_a - u_w)}{\partial t} = \frac{\partial}{\partial z} \left( \frac{k_w}{\rho_w g} \frac{\partial u_w}{\partial z} + k_w \right) - S \quad (2)$$

where  $m_v$  is the compressibility coefficient of the soil structure,  $m_w$  is the slope of the soil-water retention curve (SWRC) and  $k_w$  is the water permeability of the soil. Both  $m_w$  and  $k_w$  are highly nonlinear functions of matric suction ( $u_a - u_w$ ).  $S$  is a sink term used to model the rate of water taken out of the model through actual evapotranspiration (AET).

### Soil profiles and parameters

The geometry of two representative 1D soil models is shown in Figure 4. One-dimensional models can be used to calculate

climate-induced changes in porewater pressure within uniform slopes (Blight 1997; Li *et al.* 2005; Dijkstra and Dixon 2010), and applied to embankments and cut slopes (Fourie *et al.* 1999; Gavin and Xue 2008; Briggs *et al.* 2013a). Therefore, 1D models are also used in this study to investigate the impact of climate change on PWP regimes in clay earthworks, for the general case. The 1D models represent the mid-slope of typical railway embankments (i.e. away from the slope crest and toe) on the London Underground Ltd network (Briggs *et al.* 2013b), but do not represent the geometry of individual slopes. Each model consists of three layers: surface clay fill (1 m), clay fill (4 m) and London Clay foundation (4 m). The difference between the two models lies in the permeability of the clay fill. The saturated permeability  $k_s = 5 \times 10^{-8} \text{ m s}^{-1}$  for the clay fill in the first model is slightly greater than the median value of  $3 \times 10^{-8} \text{ m s}^{-1}$  for old clay fill embankments constructed by end tipping in the 19th century (O'Brien *et al.* 2004). In the second model, the clay fill permeability  $k_s = 5 \times 10^{-9} \text{ m s}^{-1}$  is likely to be a lower bound for old clay fill embankments (O'Brien *et al.* 2004) and has the same order of magnitude as the *in situ* London Clay (Chandler *et al.* 1990) and modern well-compacted embankments. In both models the fill is underlain by London Clay with  $k_s = 5 \times 10^{-9} \text{ m s}^{-1}$ . Therefore the lower permeability model in Figure 4 could also be taken as representative of some clay highway embankments and some clay cuttings. The surface clay layer is assigned a higher permeability  $k_s = 5 \times 10^{-7} \text{ m s}^{-1}$ , which captures the increase in permeability at the near surface of earthworks owing to weathering and desiccation cracking (Dixon *et al.* 2019). The desiccation crack depths reported by Yu *et al.* (2021) from a long-term field monitoring of a clay fill embankment in Northumberland (UK) were generally less than 0.3 m and did not exceed 1 m, which justifies the use of 1 m as an upper bound for the depth of the surface clay fill. As the clay fill of the first model is 10 times more permeable than that in the second model, the two models are hereafter referred to as the higher permeability (HP) and lower permeability (LP) model, respectively. Briggs *et al.* (2013a) showed that clay embankments underlain by a much more permeable material (e.g. chalk or river terrace deposits) can maintain low PWPs even after long wet periods, and therefore are not considered in this study. Similarly, freer draining embankments and cuttings are not considered.

The soil properties are summarized in Table 2 and the hydrological properties are illustrated in Figure 5. The SWRC for London Clay is based on the measurements by Crony (1977) and used by Briggs *et al.* (2013b, 2016). The SWRC for the clay fill was assigned a lower air-entry value and shallower gradient than the *in situ* London Clay, reflecting its greater specific volume and wider range of pore sizes (Loveridge *et al.* 2010; Briggs *et al.* 2013a, 2016). Unsaturated permeability was estimated from the SWRC in conjunction with saturated permeability using the method of Mualem (1976). The soils were assumed to be slightly compressible with  $m_v = 5 \times 10^{-5} \text{ kPa}^{-1}$  after Bell (1992).

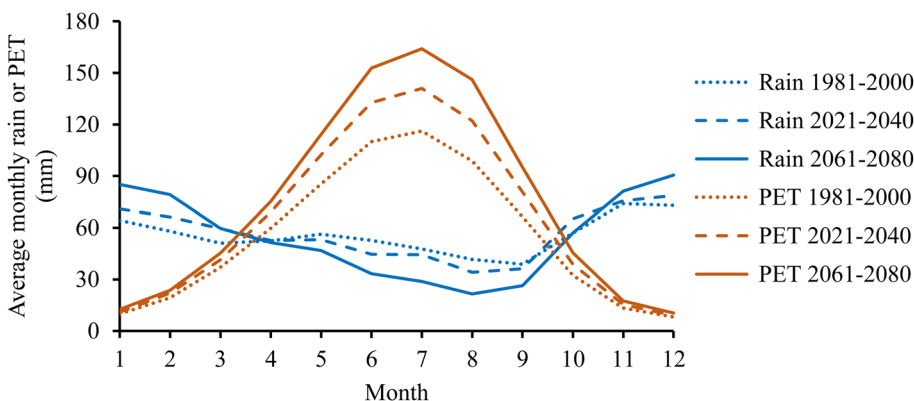
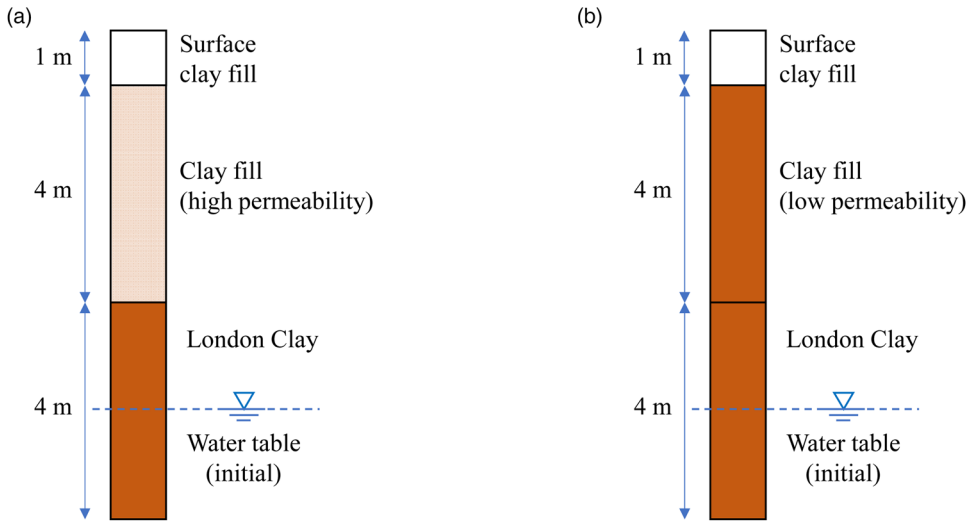


Fig. 3. Average monthly rainfall and PET from UKCP18 local projections for London Heathrow (the values shown are average of the 12 PPEs).



**Fig. 4.** Representative 1D models with high- and low-permeability clay fill. (a) Higher permeability (HP); (b) lower permeability (LP). Source: adapted from Briggs *et al.* (2013a).

**Table 2.** Summary of soil properties used in the finite-element model (data from Briggs *et al.* 2016)

	SWRC parameters (Van Genuchten 1980)				Saturated permeability $k_s$ ( $\text{m s}^{-1}$ )	Compressibility coefficient $m_v$ ( $\text{kPa}^{-1}$ )
	$\alpha$ (kPa)	$M$	$n$	$\theta_s$		
Surface clay fill	30.3	0.13	1.15	0.47	$5 \times 10^{-7}$	$5 \times 10^{-5}$
Clay fill (high permeability)	30.3	0.13	1.15	0.47	$5 \times 10^{-8}$	$5 \times 10^{-5}$
Clay fill (low permeability)	30.3	0.13	1.15	0.47	$5 \times 10^{-9}$	$5 \times 10^{-5}$
London Clay	125	0.15	1.18	0.47	$5 \times 10^{-9}$	$5 \times 10^{-5}$

### Soil–vegetation–atmosphere-transfer modelling

The soil–vegetation–atmosphere-transfer (SVAT) across the ground surface was modelled using the land climate interaction (LCI) boundary condition in SEEP/W. The required input parameters of rainfall and PET v. time were obtained from the UKCP18 local projections (directly for rainfall, and indirectly for PET via equation 1). AET depends on PET and water availability within the soil, and was calculated through a root water uptake model. The variation in key parameters is illustrated in Figure 6. The rate of root water uptake  $S$ , shown in equation (2), is limited when the soil is very wet owing to oxygen deficiency or when it is dry owing to a lack of available water. Hence,  $S$  can be related to soil suction, and the relationship suggested by Feddes *et al.* (1978) was adopted, with the anaerobiosis point  $\psi_{an} = 0$  kPa, limiting point  $\psi_l = 100$  kPa and wilting point  $\psi_w = 1500$  kPa. The root density was assumed to decrease linearly with depth (Indraratna *et al.* 2006; Tsiamposi *et al.* 2017). Two types of vegetation are considered here: grass and tree cover. It should be noted that PET is controlled by the evaporative demand of the atmosphere rather than an active

physiological function of plants (Hillel 2004). According to Biddle (1998), more than 99% of water taken up by plants is lost as transpiration, whereas less than 1% goes into direct growth. Therefore, it is reasonable to assume that grass and trees have the same PET, and their difference lies in the rooting depth. It should be noted that the distribution in Figure 6b represents the *in situ* plant water abstraction with depth rather than the actual root biomass (Leung *et al.* 2015). The root depth is set to be 0.9 m deep for grass (Briggs *et al.* 2013b) and 3 m deep for trees (Briggs *et al.* 2016) based on field measurements (Biddle 1998).

### Parametric studies

The vertical height of the 1D model was 9 m, and it was discretized into 90 equal elements of size 0.1 m. The 1D model is very computationally efficient. Therefore, the 12 PPEs from UKCP18 local projections were all used as LCI boundary conditions in the seepage analyses with rainfall and PET input at daily resolution. The base boundary was set to be impermeable, so water could only go in or out of the top of the model. The initial water table was set to be

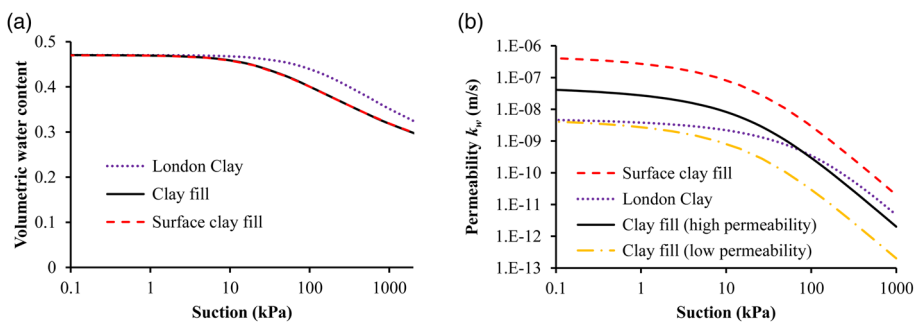


**Fig. 5.** Hydrological properties of the soils. (a) Soil–water retention curve (SWRC); (b) permeability function. Source: adapted from Briggs *et al.* (2013b).

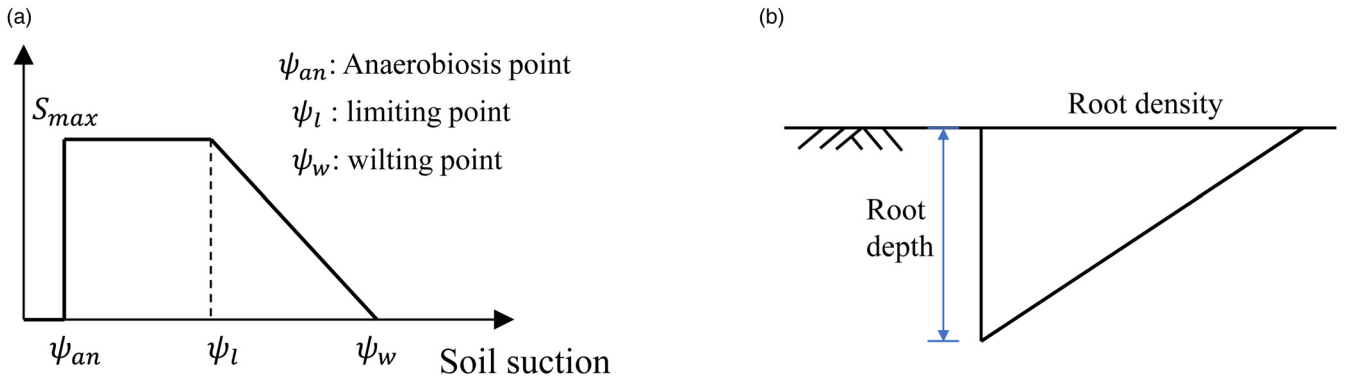


Fig. 6. Variation in key vegetation parameters. (a) Rate of root water uptake and soil suction; (b) root density distribution.

Table 3. Summary of combination of factors in the finite-element seepage analyses

Ground model	Climate data	Time period	Vegetation type	Number of combinations
HP model	12 PPEs at daily resolution from UKCP18 local projections	1981–2000	Grass	144 (= 2 × 12 × 3 × 2)
LP model		2021–2040	Trees	
		2061–2080		

7 m below ground surface (Fig. 4) with initial PWP hydrostatic relative to the water table. The same initial condition is used for each of the three time periods 1981–2000, 2021–2040 and 2061–2080. It should be noted that the initial PWP condition can have a significant influence on model results over a short period (from days to months; e.g. Rahimi *et al.* 2011). A 20 year period is modelled here, and for most of the models the water table returns to slope surface in the first few years. Therefore, the initial PWP condition may affect the model results before it reaches full saturation, but will be minimal afterwards. The effect of climate change is evaluated by comparing the results for 2021–2040 or 2061–2080 relative to those for 1981–2000 (baseline), and therefore the initial PWP condition has negligible influence on the outputs of interest. It is admitted that a simple 1D model may not be as accurate as a more advanced (e.g. multidimensional coupled) model. However, because the simple model is used with both the baseline and projected climate data, the right trend in the effects of climate change is captured. In the SVAT modelling, either grass or tree cover is considered. As summarized in Table 3, a total of 144 analyses were carried out.

### Key indicators to interpret the seepage analysis results

The key indicators used to interpret water balance and PWP conditions from the seepage analyses are explained first below, and the results are then presented below.

#### Cumulative net infiltration and water storage capacity

Net infiltration (NI) can be calculated as the balance of rainfall (P), actual evapotranspiration (AET) and runoff (RO) (e.g. Pk *et al.* 2021; Bashir *et al.* 2022),

$$NI = P - AET - RO \quad (3)$$

and the cumulative net infiltration (CNI) can be calculated as

$$CNI = \sum P - \sum AET - \sum RO \quad (4)$$

where  $\sum$  denotes a summation with time. The value of CNI is positive to describe net infiltration and negative to describe net evapotranspiration. CNI quantifies the amount of water entering or leaving the soil. The former leads to an increase in PWP and the latter to a decrease in PWP. CNI can be linked to the worst-case (i.e.

maximum) PWP together with a parameter that defines the amount of space in the soil that is able to store water. Soil moisture deficit (SMD) is commonly used to quantify the volume of water required to return the soil profile to close to a saturated state. However, the calculation of SMD is often limited to the root zone (e.g. Smethurst *et al.* 2012). A modified SMD is proposed here, in which the moisture deficit is evaluated within the vadose zone (down to the phreatic surface) rather than being limited to the root depth. To avoid confusion with SMD, the parameter is called water storage capacity (WSC) and can be calculated as

$$WSC = \int (\theta_s - \theta_i) dz \quad (5)$$

where  $\theta_s$  is the saturated volumetric water content,  $\theta_i$  is the initial volumetric water content and  $z$  denotes the elevation in the unsaturated zone. Both CNI and WSC should be considered relative to a point in time according to their definitions. For comparative purposes, they should be taken relative to the same time point, and the initial condition of the seepage analysis ( $t = 0$ ) is adopted in this study. The relation between CNI, WSC and PWP can then be stated as follows: when CNI equals WSC, the water table is raised to slope surface representing the maximum or worst-case PWP condition.

The WSC relative to  $t = 0$  depends on the initial PWP profile and the SWRC of the soil, and as the two models shown in Figure 4 have the same initial PWP profiles and SWRCs, the WSC of the two models is the same. The WSC of the three soil layers calculated by equation (5) are shown in Figure 7. The WSC for the London Clay foundation is only 7 mm, as the average suction in the London Clay is 10 kPa, which is significantly below the air-entry value, and therefore the soil at initial condition is already close to full saturation. The WSC for the clay fill and surface clay fill are 149 and 54 mm, respectively. The total WSC of the three soil layers is therefore 210 mm.

The change of CNI with time is illustrated by an example shown in Figure 8a. The seepage analysis was carried out for the HP model (Fig. 4a) with the wettest PPE (Member 1113) and grass cover. In Figure 7 the total soil volume is assumed not to change with time; that is, the soils are incompressible ( $m_v = 0$ ), and therefore  $WSC = 0.21$  m. In the seepage analysis, some compressibility of the soils was considered ( $m_v = 5 \times 10^{-5} \text{ kPa}^{-1}$ ; refer to Table 2). The soil volume expands when the water is in a compressive state (i.e. PWP is positive), and  $WSC = 0.23$  m in the seepage analysis. When the CNI

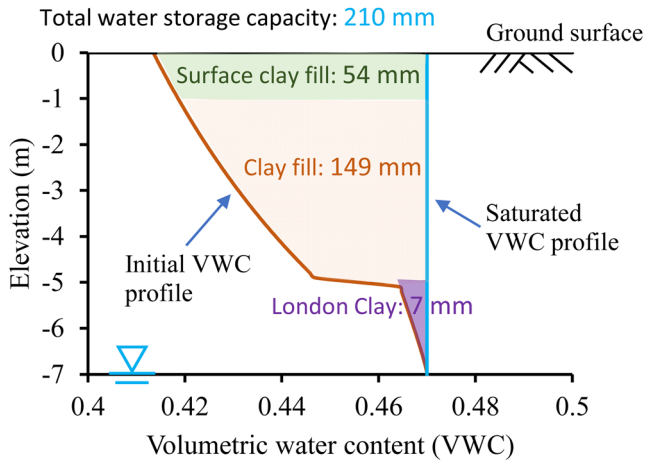


Fig. 7. Water storage capacity of the ground model (relative to initial condition  $t = 0$ ).

equals the WSC, the soil profile is completely saturated and the water table is raised to ground surface, which is the worst PWP condition possible for geotechnical stability analysis. In this situation there is no remaining water storage capacity, further rainfall infiltration is not possible and additional rainfall becomes runoff.

### Hydrostatic ratio

The porewater pressure (PWP) condition is often interpreted through a porewater pressure profile plotted with depth (Zhang

*et al.* 2004; Smethurst *et al.* 2006, 2012; Lee *et al.* 2009; Briggs *et al.* 2013a). The outermost of the PWP profiles, also known as the PWP envelope, is often selected as the design condition (e.g. Lee *et al.* 2009). Each seepage analysis in this study (summarized in Table 3) was carried out for a 20 year period at a daily time step. The worst-case PWP (i.e. the water table reaching the slope surface) can occur for most of the models, although the frequency of occurrence is different and can be affected by soil permeability, vegetation cover and climate change.

To evaluate the frequency of worst-case PWP, each PWP profile needs to be examined. A total of 1 032 480 (>1 million) PWP profiles were generated in the seepage analyses in this study. Interpreting each PWP profile visually and manually would not be feasible. Therefore, an index is proposed to quantify the PWP condition. To avoid confusion with the PWP ratio proposed by Bishop and Morgenstern (1960), the index is called hydrostatic ratio ( $H_r$ ). The definition of  $H_r$  is illustrated in Figure 9, and  $H_r$  is calculated as

$$H_r = \frac{A_1}{A_2} \quad (6)$$

where  $A_1$  is the area enclosed by the PWP at a given time (where the area in which PWP is below zero is taken as negative) and  $A_2$  is the area enclosed by the hydrostatic PWP (positive).

An example of  $H_r$  calculated using equation (6) is shown in Figure 8b. Good agreement is shown between the trends of CNI in Figure 8a and  $H_r$  in Figure 8b. When CNI approaches the WSC,  $H_r$  also approaches unity. The theoretical value of  $H_r$  is equal to unity when the water table is at the ground surface. It should be noted that

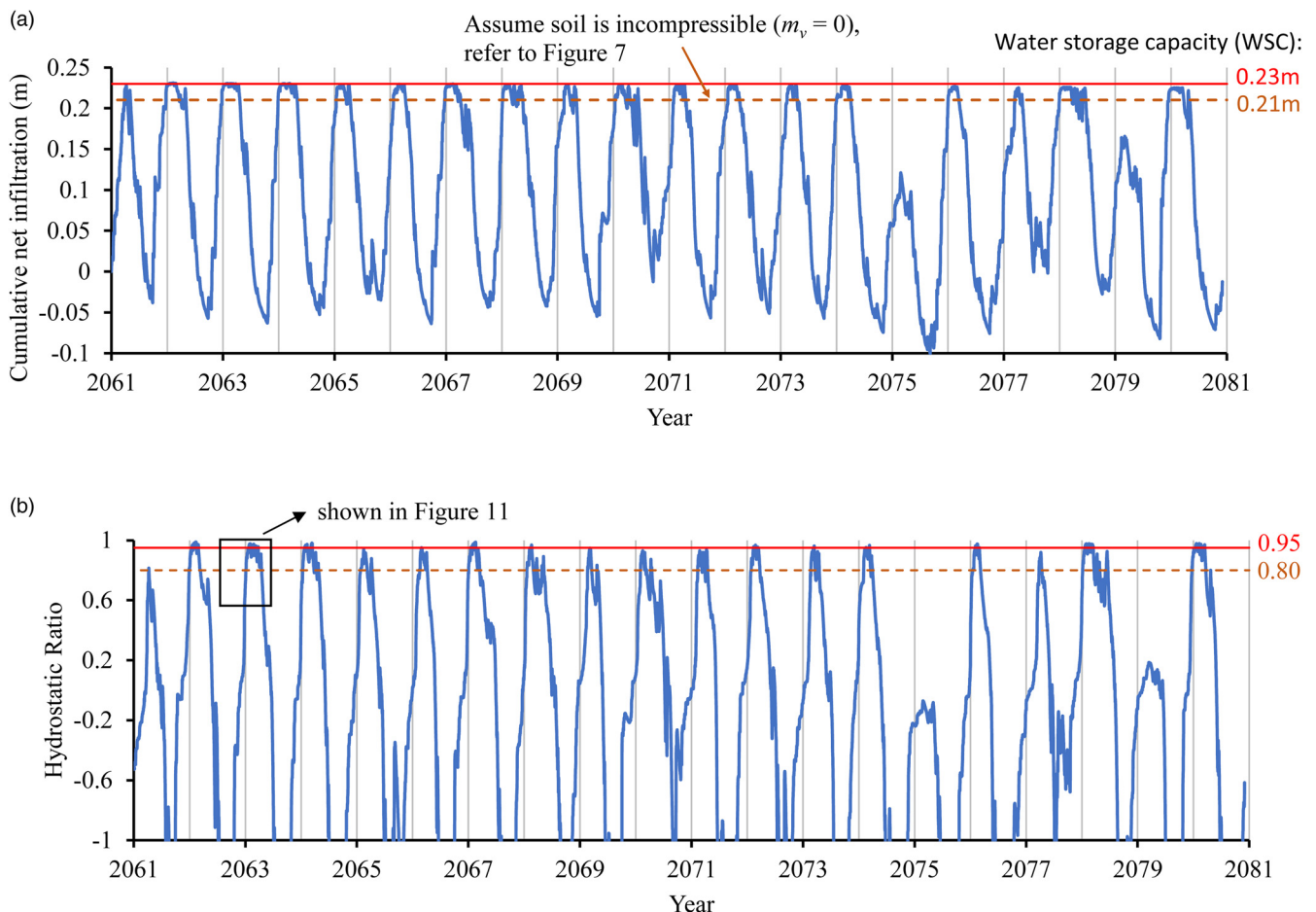
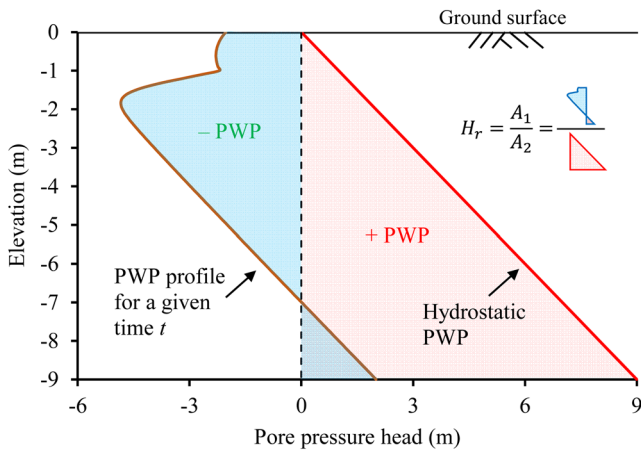


Fig. 8. Use of cumulative net infiltration, water storage capacity (WSC) and hydrostatic ratio to interpret the porewater pressure (PWP) conditions (HP model with grass cover, climate data from PPE member 1113). (a) Cumulative net infiltration (defined by equation (4)); (b) hydrostatic ratio (defined by equation (6)).





**Fig. 9.** Definition of hydrostatic ratio  $H_r$  (calculated as the ratio of the areas enclosed by the PWP profiles and  $H_r$  can be negative).

the maximum  $H_r$  computed from the finite-element seepage analysis is often slightly less than unity (e.g. 0.997 in Fig. 8b) owing to numerical error.  $H_r = 0.95$  and  $0.80$  are indicated in Figure 8b, and the corresponding equivalent linear PWP profiles are shown in Figure 10. It should be noted that the PWP profiles for  $H_r = 0.95$  and  $0.80$  are not unique, but are indicators that groundwater level is approaching the slope surface. In the seepage analysis, the  $H_r$  for each day can be calculated. A ‘wet day’ is defined here as a day on which a threshold value of  $H_r$  (e.g.  $0.80$ ,  $0.95$ ) is exceeded. It should be noted that the threshold adopted can affect the number of wet days counted, as revealed in Figure 8b and more clearly shown in Figure 11. There are 23 wet days for the given period if the criterion  $H_r \geq 0.95$  is adopted, and 101 wet days for the criterion  $H_r \geq 0.80$ . By using the proposed hydrostatic ratio, the large number of PWP profiles (>1 million) can readily be quantified, and further statistical analysis carried out. The impact of climate change on the frequency of the worst-case PWP is discussed in more detail below.

## Results

All the 12 PPEs from UKCP18 local projections were used in the seepage analyses. For each PPE, seepage analyses were carried out corresponding to three periods (1981–2000, 2021–2040 or 2061–2080), two soil permeabilities (HP and LP models) and two vegetation types (grass or tree cover), as summarized in Table 3. For each period, soil permeability and vegetation type, the results can be interpreted (1) as the average of the 12 seepage analyses corresponding to the 12 PPEs or (2) by plotting the 12 sets of results as boxplots. The results related to the water balance and

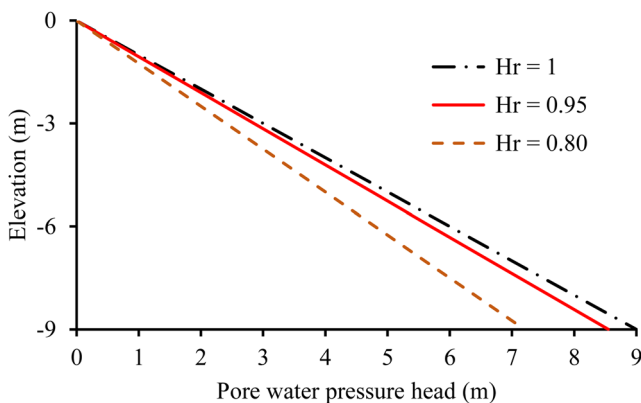


**Fig. 10.** Illustration of porewater pressure profiles for hydrostatic ratio ( $H_r$ ) thresholds.

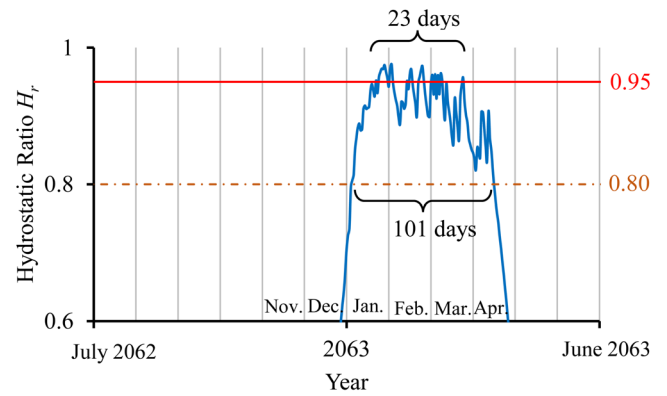


**Fig. 11.** Determination of the number of wet days; an example (HP model with grass cover, climate data from PPE member 1113).

porewater pressure condition are presented below using the key indicators described in the previous section.

## Water balance

Analysis of the projected climate data (Fig. 3) showed greater PET and less rainfall in summer and more rainfall in winter. To clearly see this seasonality, the results should be interpreted by dry/wet seasons or by months. A typical result is shown in Figure 12 for the change of monthly water balance at three time periods 1981–2000, 2021–2040 and 2061–2080 for the HP model (Fig. 12a–c) and LP model (Fig. 12d–f) with grass cover. In the early summer (April to June), climate change causes a significant increase in AET (owing to the higher PET), negligible change in runoff and significant increase in net evapotranspiration (owing to the combination of higher AET and less rainfall). In the late summer (July to September), it is interesting that the AET for 2061–2080 is the lowest (owing to the limited water availability) even though the PET is the highest among the three periods. However, the change of NI is limited, as both rainfall and AET decrease. In the mid-winter (December, January and February), there is a significant increase of NI for the HP model with grass cover (Fig. 12c) because of the increase in winter rainfall. However, the increase of NI for the LP model with grass cover is not obvious (Fig. 12f), as the infiltration rate is governed by the soil permeability, and the increase in rainfall intensity leads to more runoff (Fig. 12e). For the other winter months (October, November and March), there is little difference between 2061–2080 and 1981–2000 in terms of rainfall, AET and runoff, and therefore NI is also about the same. The changes in water balance for the HP and LP models with tree cover are similar to those in Figure 12 and therefore are not shown.

As discussed above and shown in Figure 8, CNi can be linked to changes in PWP. Therefore, the impact of climate change on CNi is comprehensively investigated. Based on the characteristics of NI (Fig. 12c and f) and to capture the seasonality, each year is divided into four periods: early summer (Apr, May, Jun), late summer (Jul, Aug, Sep), mid-winter (Dec, Jan, Feb) and the other winter months (Oct, Nov, Mar). For a given PPE and seepage analysis, seasonal CNi can be calculated and taken as average for the 20 years (1981–2000, 2021–2040 or 2061–2080). The seasonal CNis from the 12 seepage analyses for each soil permeability and vegetation cover are shown in Figure 13 as boxplots. In the early summer, there is clear increase in net evapotranspiration with time for all the models. In the mid-winter, for the HP model there is clear increase in net infiltration over time (Fig. 13a and b), but for the LP model the increase is not as obvious and the net infiltration is also not much different from that for the other winter months. The HP model has higher clay fill permeability, and therefore the net infiltration can be

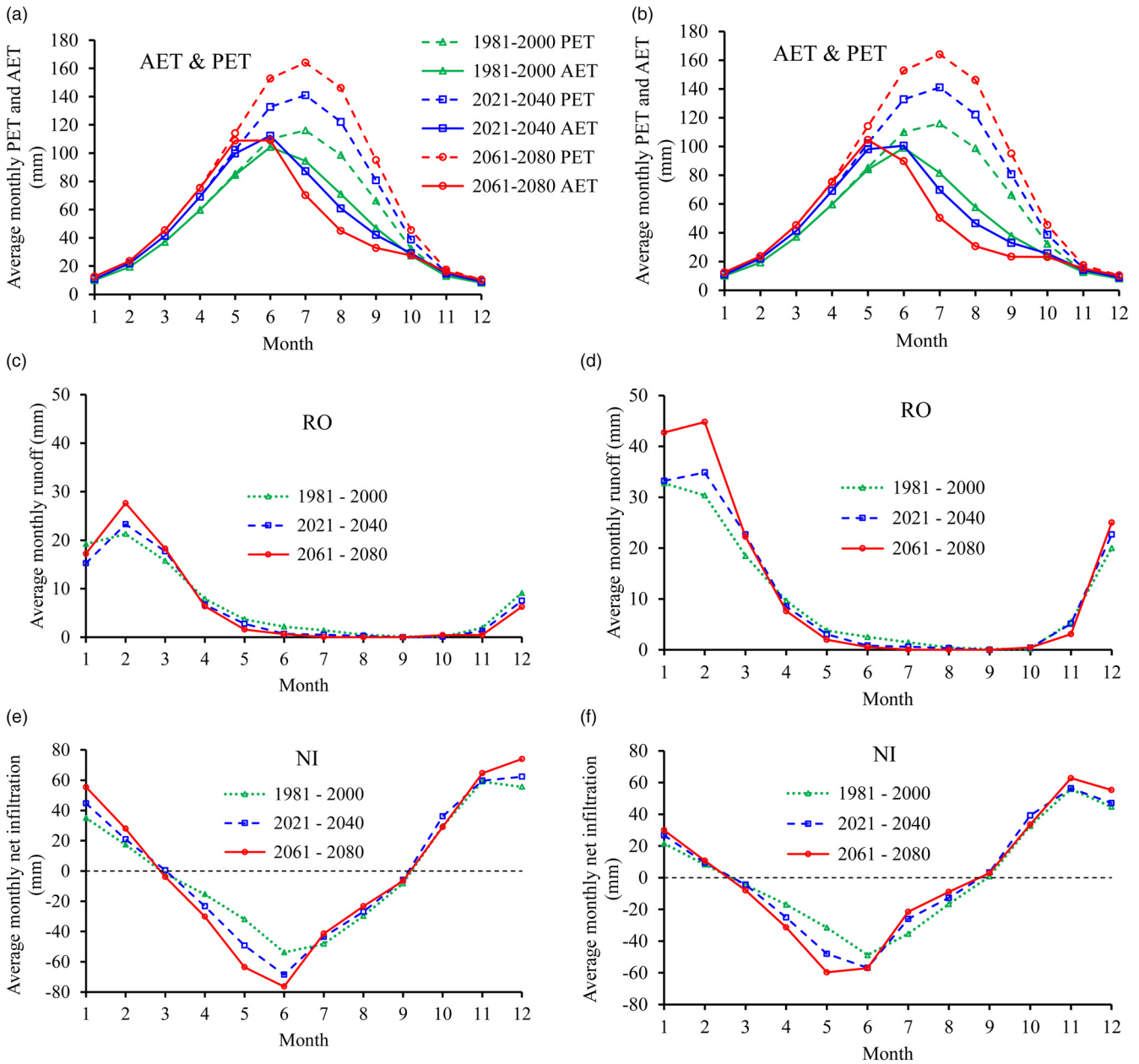


**Fig. 12.** Water balance (the values shown are average outputs from the 12 simulations): (a–c) HP model with grass cover; (d–f) LP model with grass cover.

affected by rainfall intensity. The LP model has lower clay fill permeability, which governs the infiltration rate, and the increase in rainfall intensity has little effect. The main difference between slopes with grass cover and tree cover lies in the net evapotranspiration in the late summer. For slopes with tree cover, the roots are deeper, therefore significant AET can take place even though the soil has limited water availability in late summer.

As well as the absolute magnitude of CNI, the size of the annual dry–wet cycles is also critical to slope stability, as they are directly related to shrink–swell behaviour and can drive deterioration in higher plasticity materials such as London Clay (Rouainia *et al.* 2020; Postill *et al.* 2021). Clarke and Smethurst (2010) investigated the effects of climate change (using UKCIP02) on dry–wet cycles using an SMD-based soil water balance model. Their research is advanced in this study by using the more rigorous FE-based SVAT modelling and use of UKCP18. The values of cumulative difference of rainfall and PET (i.e. rainfall – PET) for summer (April to September) and winter (October to March) are calculated to quantify dryness and wetness, respectively. The absolute sum of

these values gives a cycle size based on the climate boundary. The dry–wet cycle can also be quantified through the soil response by replacing (rainfall – PET) with seasonal CNI, which takes into account the soil–vegetation–atmosphere interaction. Table 4 shows the average annual dry–wet cycles for both definitions, and the values shown are taken as averages for 20 years and from 12 PPEs or seepage analyses. Therefore, the values shown in Table 4 represent only the average scenario and do not capture the extremes (Huang *et al.* 2023). The values are negative for summer and positive in winter, and show clear changes in seasonality and in cycle size for the three time periods (1981–2000, 2021–2040 and 2061–2080). The climate boundary summer drying increases substantially, with smaller changes in winter wetting, consistent with Figure 3. When considering the soil response, the actual drying obtained is reduced. However, it still increases in future decades, as does the soil wetting in winter. Therefore the cycle size increases between 17 and 42% depending on the soil permeability and vegetation type. The greatest impact is seen with the HP soil and trees, which both facilitate deeper drying.

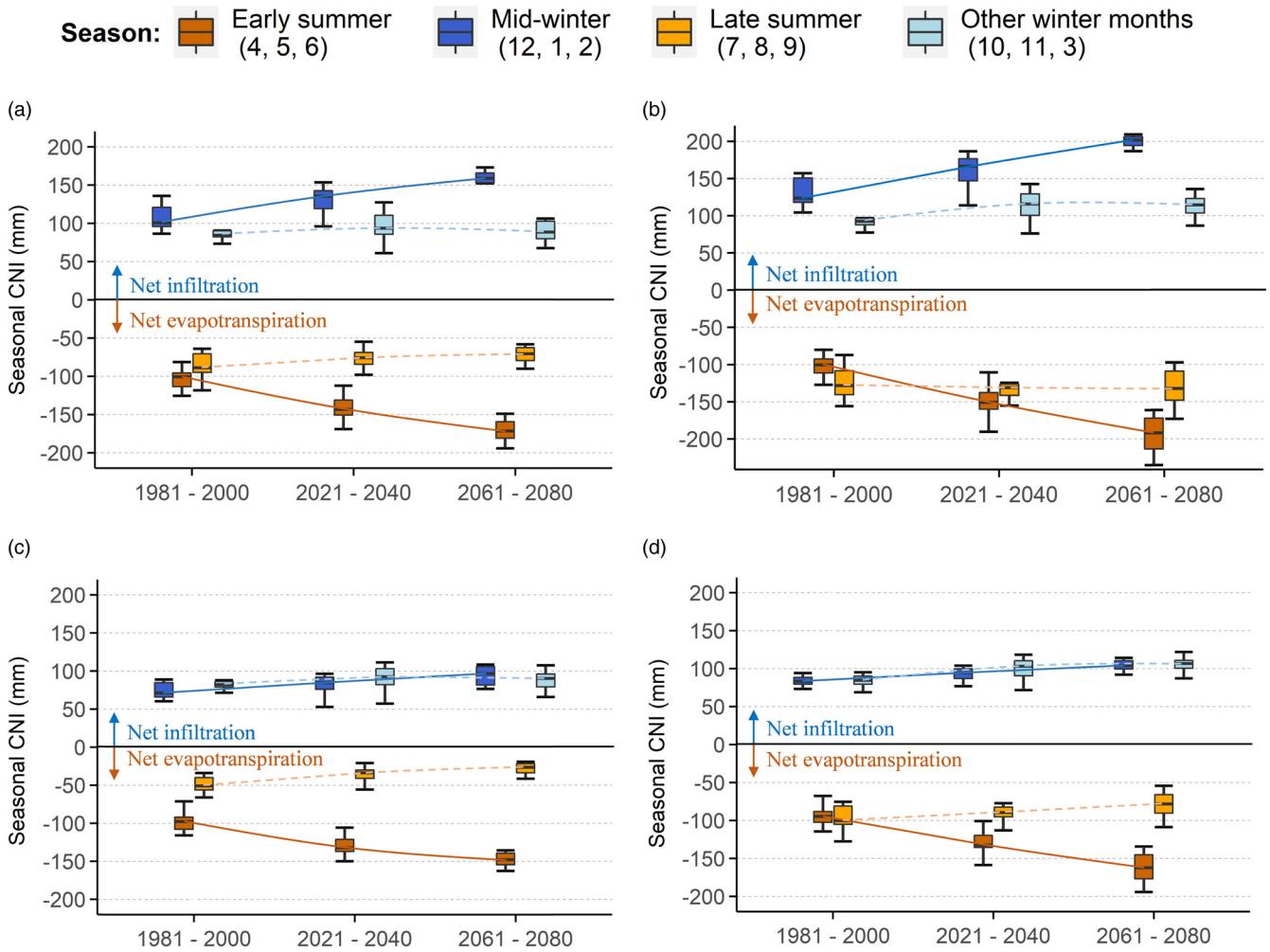


Fig. 13. Change of seasonal cumulative net infiltration (CNI) with time (shown as boxplots representing 12 simulations). (a) HP model – grass cover; (b) HP model – tree cover; (c) LP model – grass cover; (d) LP model – tree cover.

### Frequency of the occurrence of worst-case porewater pressure

The worst-case PWP scenario for slope stability analysis is when water table is at the slope surface. This has been quantified by use of the  $H_r$  criterion (as described above) to determine the number of ‘wet days’, defined as when the water table approaches the slope surface. It should be noted that the threshold adopted for  $H_r$  can affect the number of wet days counted, as shown in Figure 11. If there is at least one wet day in a year, that year is now also called a ‘wet year’. The frequency of the occurrence of worst-case PWP can

be examined in terms of the number of wet days per month or year and the number of wet years in a 20 year period, as discussed below. Figures 14 and 15 show this information for the HP model with grass cover. Because of space constraints, results for the other models are not shown. In general, the number of wet days decreases with the projected climate change.

The numbers of wet years in the three 20 year periods 1981–2000, 2021–2040 and 2061–2080 are shown in Figure 16. For slopes with a grass cover, the wet year frequency slightly decreases, but a wet year still occurs often enough that water table at the ground surface should be considered as the worst credible scenario. For the

Table 4. Impact of climate change on annual dry (summer) and wet (winter) cycles

	Average (rainfall with PET) (mm)			Average net infiltration (mm) (HP model with grass cover)			Average net infiltration (mm) (HP model with tree cover)		
	Summer	Winter	Size of cycle	Summer	Winter	Size of cycle	Summer	Winter	Size of cycle
1981–2000	–247	257	504	–187	194	381	–225	224	449
2021–2040	–383 (55%)	279 (8%)	662 (31%)	–218 (16%)	223 (15%)	441 (16%)	–282 (25%)	275 (23%)	557 (24%)
2061–2080	–539 (119%)	298 (16%)	837 (66%)	–242 (29%)	246 (27%)	488 (28%)	–325 (44%)	313 (40%)	638 (42%)
	Average net infiltration (mm) (LP model with grass cover)			Average net infiltration (mm) (LP model with tree cover)					
	Summer	Winter	Size of cycle	Summer	Winter	Size of cycle			
1981–2000	–149	158	306	–192	169	361			
2021–2040	–165 (11%)	174 (10%)	339 (11%)	–221 (15%)	194 (15%)	415 (15%)			
2061–2080	–176 (18%)	183 (16%)	359 (17%)	–241 (25%)	211 (25%)	452 (25%)			

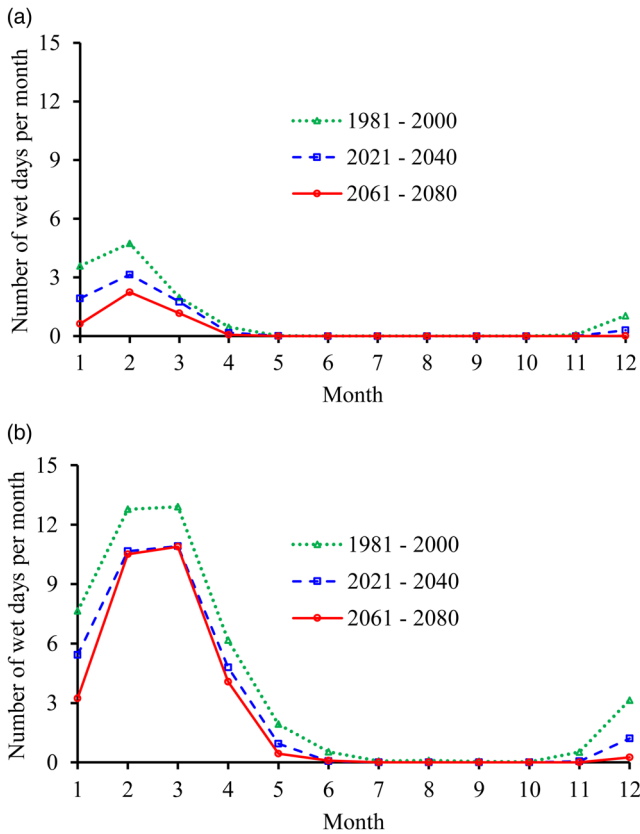


**Fig. 14.** Average number of wet days per month for HP model with grass cover (the values shown are average outputs from 12 simulations). (a) Hydrostatic ratio criteria 0.95; (b) hydrostatic ratio criteria 0.8.

HP model with tree cover, AET is more effective than for the grass cover in the future periods owing to a greater rooting and water abstraction depth, and the wet year frequency decreases significantly. For the LP model with tree cover, the saturated permeability of the clay fill is low ( $k_v = 5 \times 10^{-9} \text{ m s}^{-1}$ ). The permeability is decreased further as suctions are generated by the trees, and becomes sufficiently low that it almost prevents rainfall infiltration, meaning that there are no wet years (as defined by  $H_r \geq 0.80$ ).

**A conceptual framework on the impact of climate change**

Figure 17 shows a conceptual framework for the impact of climate change on the hydrological response of a slope to summer and winter weather conditions. The projected climate (Fig. 3) shows that the PET will increase significantly. As a result, slopes will become

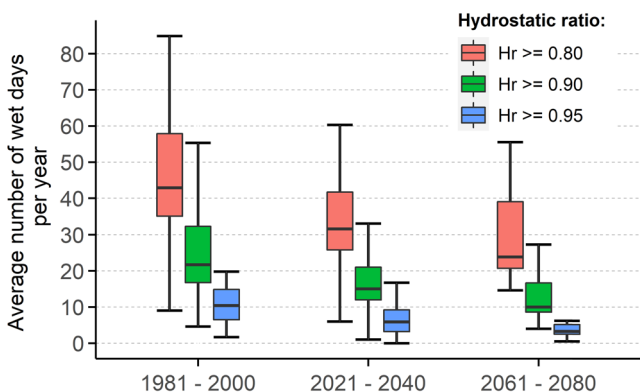


**Fig. 15.** Average number of wet days per year from 12 simulations for HP model with grass cover.

drier owing to greater net evapotranspiration, creating more water storage capacity. The magnitude of net evapotranspiration can be affected by vegetation type, with deeper roots allowing greater transpiration even when soil water is limited in the late summer. In winter, the change of PET is negligible, yet rainfall increases significantly. The greater water storage created in summer has two consequences. First, there is more net infiltration if the infiltration rate is governed by rainfall intensity, but net infiltration may not increase if the infiltration rate is limited by the soil permeability. Second, there is a greater soil pore space that needs to be refilled with water. Consequently, it takes a longer time to bring the water table to the slope surface, and therefore the worst-case PWP occur less frequently.

**Implications for earthworks design and management**

This study was carried out for earthworks made of clay fill and/or *in situ* clay with a relatively low permeability ( $5 \times 10^{-8}$  to  $5 \times 10^{-9} \text{ m s}^{-1}$ ) using climate projections for the London area. Although the 1D model used in this study is simple, the conceptual framework derived is useful to understand the physical impact of climate change on earthworks and the insights could be further examined with more sophisticated coupled models. The implications for earthwork design are listed below.

- The projected climate change is not expected to require higher design PWPs for analysis of deep-seated slips. A localized perched water table at shallow depth (owing to weathering, desiccation cracking, etc.) is expected even with the current climate (Smethurst *et al.* 2006, 2012).
- Climate change will lead to increases in the magnitude of dry–wet cycles. This will drive greater shrink–swell behaviour, and may increase desiccation cracking. This also means that the rate of weather-driven deterioration of soil strength is likely to increase.
- For clay slopes of low permeability, the infiltration rate is governed by the soil permeability. Therefore, the increase in rainfall intensity leads to significantly increased runoff. This may bring challenges to drainage management and potentially cause more flooding or erosional failures such as washout, in both clays and other materials.
- The projected increase of PET will have a greater impact for slopes with tree cover than for those with grass cover, as trees have deeper roots and can transpire water even in the late summer when the availability of soil water is limited. Therefore, the vegetation management strategy of earthworks (Briggs *et al.* 2013b; Smethurst *et al.* 2015) needs to be reviewed in the context of climate change.

A comprehensive global review by Gariano and Guzzetti (2016) concluded that climate change could increase the risk of shallow landslides and debris flows, but the risk of deep-seated landslide may decrease or show no significant change. This conclusion is also supported by this study.

**Conclusions**

This study investigated the impact of climate change on porewater pressures (PWPs) for clay earthwork design. The latest national climate projections (UKCP18) at the finest local scale (2.2 km) were used, based on a location in London. The highest carbon emission scenario (RCP8.5) was applied using 12 perturbed parameter ensembles (PPEs) to capture the widest possible scenarios of climate change. The key findings are summarized below.

- (1) The projected climate showed that there will be more potential evapotranspiration (PET) and less rainfall in

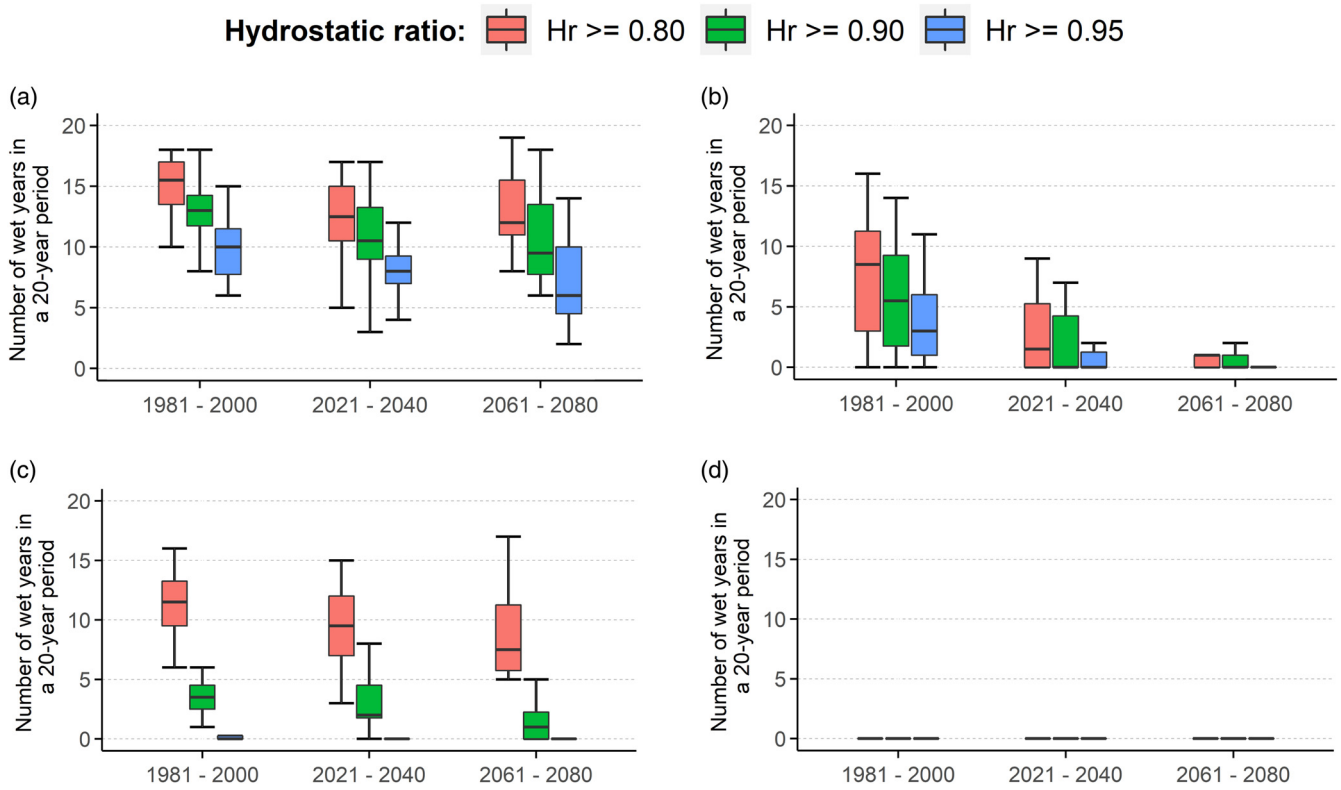


**Fig. 16.** Number of wet years in a 20 year period in 1981–2000, 2021–2040 and 2061–2080 from 12 simulations. (a) HP model – grass cover; (b) HP model – tree cover; (c) LP model – grass cover; (d) LP model – tree cover.

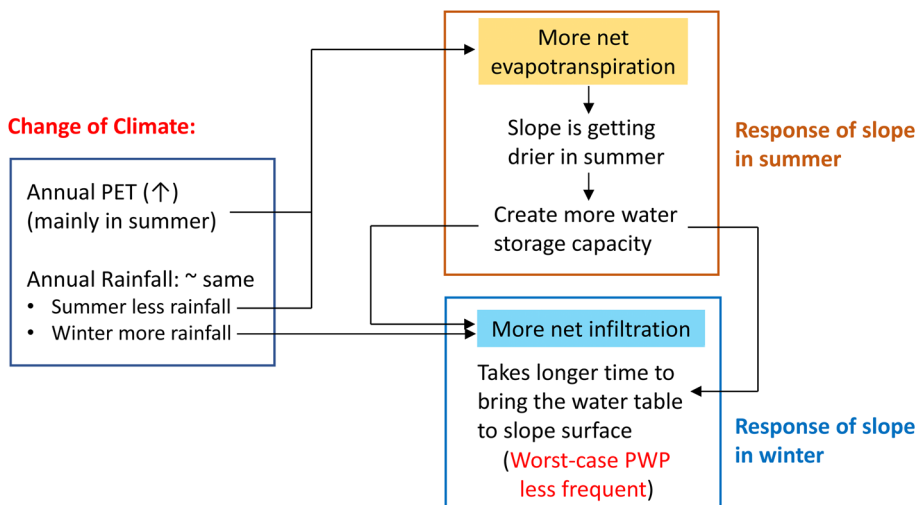


**Fig. 17.** Change of climate and slope response in summer and winter.

summer and more rainfall in winter. It is important to consider both precipitation and PET to forecast the effects of climate change, as the moisture deficit created in the dry season can affect the water balance and PWP development in the wet season.

- Owing to the higher net evapotranspiration and greater water storage capacity created in summer, it takes a longer time to refill the soil pores with rainwater in winter. Therefore, worst-case design PWPs for deep-seated slips are expected to occur less often, but a localized perched water table could continue to develop at shallow depth. In the future, design PWPs in clay earthworks are unlikely to be higher with climate change.
- The magnitude of dry–wet cycles will increase in the future, by up to 42% depending on the soil and vegetation conditions. This will potentially increase the rate of strength

deterioration in strain softening clay materials, increasing vulnerability to slope failures even if PWP conditions do not worsen.

- The magnitude and spatial extent of dry–wet cycles driven by climate change will be greater where there is tree cover compared with slopes with grass cover, as trees have deeper roots and can transpire water even in the late summer when the availability of water becomes limited.
- Although slopes with lower permeability will see a smaller increase in dry–wet cycle magnitude, the increase of rainfall intensity will cause greater surface runoff, with consequences for flood risk and erosional failures.
- Climate and climate changes projections are site specific. Although the conclusions presented above are specific to one location, it is expected that the trends may be relevant for elsewhere in the UK. The modelling, interpretation

method and conceptual framework (Fig. 17) developed in this study can also be used (or adapted) for other sites.

*Scientific editing by Colin Serridge*

**Acknowledgements** The authors would like to acknowledge assistance from Professor C. Kilsby and thank Dr D. Hughes and Professor R. Moore for reviewing and providing constructive comments on this paper.

**Author contributions** **WH:** conceptualization (equal), data curation (equal), investigation (lead), methodology (lead), validation (lead), visualization (lead), writing – original draft (lead), writing – review & editing (lead); **FAL:** conceptualization (equal), data curation (equal), funding acquisition (equal), methodology (supporting), project administration (lead), supervision (lead), writing – original draft (supporting), writing – review & editing (supporting); **KMB:** funding acquisition (equal), supervision (supporting), writing – review & editing (equal); **JAS:** funding acquisition (equal), supervision (supporting), writing – review & editing (supporting); **NS:** writing – review & editing (supporting); **FT:** writing – review & editing (supporting)

**Funding** The authors are grateful for the financial support of the Engineering and Physical Sciences Research Council (EPSRC) through the programme Grant ACHILLES (EP/R034575/1). K.B. is supported by the Royal Academy of Engineering (RCSRF1920/10/65) and HS2 Ltd under the Senior Research Fellowship scheme.

**Competing interests** The authors declare that they have no known competing financial interests or personal relationships that could have appeared to influence the work reported in this paper.

**Data availability** The UKCP18 data and historical weather data used in this study can be downloaded from <https://ukclimateprojections-uk.metoffice.gov.uk/products>. The derived results are freely available from the University of Leeds data repository (<https://doi.org/10.5518/1435>).

## References

- Allen, R.G., Pereira, L.S., Raes, D. and Smith, M. 1998. *Crop Evapotranspiration – Guidelines for Computing Crop Water Requirements – FAO Irrigation and Drainage Paper 56*. Food and Agriculture Organization of the United Nations, Rome.
- Bashir, R., Sahi, M.A. and Sharma, J. 2022. Using synthetic climate datasets for geotechnical and geoenvironmental design problems. *Canadian Geotechnical Journal*, **59**, 1305–1320, <https://doi.org/10.1139/cgj-2021-0408>
- Bell, F.G. 1992. *Engineering Properties of Soils and Rocks*, 3rd edn. Butterworth–Heinemann.
- Biddle, P.G. 1998. *Tree Root Damage to Buildings*. Willowmead, Wantage.
- Bishop, A.W. and Morgenstern, N. 1960. Stability coefficients for earth slopes. *Géotechnique*, **10**, 129–153, <https://doi.org/10.1680/geot.1960.10.4.129>
- Blight, G.E. 1997. Interactions between the atmosphere and the earth. *Géotechnique*, **47**, 715–767, <https://doi.org/10.1680/geot.1997.47.4.713>
- Booth, A. 2014. *Impacts of desiccation cracking and climate change on highway cutting hydrology*. PhD thesis, Loughborough University.
- Bormann, H. 2011. Sensitivity analysis of 18 different potential evapotranspiration models to observed climatic change at German climate stations. *Climatic Change*, **104**, 729–753, <https://doi.org/10.1007/s10584-010-9869-7>
- Briggs, K.M., Smethurst, J.A., Powrie, W. and O'Brien, A.S. 2013a. Wet winter pore pressures in railway embankments. *Proceedings of the Institution of Civil Engineers – Geotechnical Engineering*, **166**, 451–465, <https://doi.org/10.1680/jgeeng.11.00106>
- Briggs, K.M., Smethurst, J.A., Powrie, W., O'Brien, A.S. and Butcher, D.J.E. 2013b. Managing the extent of tree removal from railway earthwork slopes. *Ecological Engineering*, **61**, 690–696, <https://doi.org/10.1016/j.ecoleng.2012.12.076>
- Briggs, K.M., Smethurst, J.A., Powrie, W. and O'Brien, A.S. 2016. The influence of tree root water uptake on the long term hydrology of a clay fill railway embankment. *Transportation Geotechnics*, **9**, 31–48, <https://doi.org/10.1016/j.trgeo.2016.06.001>
- Briggs, K.M., Loveridge, F.A. and Glendinning, S. 2017. Failures in transport infrastructure embankments. *Engineering Geology*, **219**, 107–117, <https://doi.org/10.1016/j.enggeo.2016.07.016>
- Brown, M.J., Robinson, E.L., Kay, A.L., Chapman, R., Bell, V.A. and Blyth, E.M. 2022. *Potential evapotranspiration derived from HadUK-Grid 1 km gridded climate observations 1969–2021 (Hydro-PE HadUK-Grid)*. NERC EDS Environmental Information Data Centre, <https://doi.org/10.5285/9275ab7e-6e93-42bc-8e72-59c98d409deb>
- Bussière, B., Aubertin, M., Mbonimpa, M., Molson, J.W. and Chapuis, R.P. 2007. Field experimental cells to evaluate the hydrogeological behaviour of oxygen barriers made of silty materials. *Canadian Geotechnical Journal*, **44**, 245–265, <https://doi.org/10.1139/t06-120>
- Chandler, R.J., Leroueil, S. and Trenter, N.A. 1990. Measurements of the permeability of London Clay using a self-boring permeameter. *Géotechnique*, **40**, 113–124, <https://doi.org/10.1680/geot.1990.40.1.113>
- Chun, K.P., Wheatler, H.S. and Onof, C. 2012. Projecting and hindcasting potential evaporation for the UK between 1950 and 2099. *Climatic Change*, **113**, 639–661, <https://doi.org/10.1007/s10584-011-0375-3>
- Clarke, D. and Smethurst, J.A. 2010. Effects of climate change on cycles of wetting and drying in engineered clay slopes in England. *Quarterly Journal of Engineering Geology and Hydrogeology*, **43**, 473–486, <https://doi.org/10.1144/1470-9236/08-106>
- Climate Change Committee. 2021. *Independent Assessment of UK Climate Risk Advice to Government for the UK's third Climate Change Risk Assessment (CCRA3)*, June 2021. <https://www.theccc.org.uk/wp-content/uploads/2021/07/Independent-Assessment-of-UK-Climate-Risk-Advice-to-Govt-for-CCR-A3-CCC.pdf> [accessed 18 October 2022].
- Climate Change Impacts Review Group (CCIRG). 1991. *The Potential Effects of Climate Change in the United Kingdom*. HMSO, London.
- Coe, J.A. and Godt, J.W. 2012. Review of approaches for assessing the impact of climate change on landslide hazards. In: Eberhardt, E., Froese, C., Turner, A.K. and Leroueil, S. (eds) *Landslides and Engineered Slopes, Protecting Society Through Improved Understanding: Proceedings of the 11th International and 2nd North American Symposium on Landslides and Engineered Slopes*, 3–8 June, Banff, Canada. Taylor & Francis, London, **1**, 371–377.
- Collison, A., Wade, S., Griffiths, J. and Dehn, M. 2000. Modelling the impact of predicted climate change on landslide frequency and magnitude in SE England. *Engineering Geology*, **55**, 205–218, [https://doi.org/10.1016/S0013-7952\(99\)00121-0](https://doi.org/10.1016/S0013-7952(99)00121-0)
- Crone, D. 1977. *The Design and Performance of Road Pavements*. Technical report. Her Majesty's Stationery Office.
- Dixon, N. and Brook, E. 2007. Impact of predicted climate change on landslide reactivation: case study of Mam Tor, UK. *Landslides*, **4**, 137–147, <https://doi.org/10.1007/s10346-006-0071-y>
- Dixon, N., Crosby, C.J. *et al.* 2019. *In situ* measurements of near-surface hydraulic conductivity in engineered clay slopes. *Quarterly Journal of Engineering Geology and Hydrogeology*, **52**, 123–135, <https://doi.org/10.1144/qjegh2017-059>
- Dijkstra, T.A. and Dixon, N. 2010. Climate change and slope stability in the UK: challenges and approaches. *Quarterly Journal of Engineering Geology and Hydrogeology*, **43**, 371–385, <https://doi.org/10.1144/1470-9236/09-036>
- Dodman, D., Hayward, B. *et al.* 2022. Cities, settlements and key infrastructure. In: Pörtner, H.-O., Roberts, D.C. *et al.* (eds) *Climate Change 2022: Impacts, Adaptation and Vulnerability. Contribution of Working Group II to the Sixth Assessment Report of the Intergovernmental Panel on Climate Change*. Cambridge University Press, Cambridge, 907–1040, <https://doi.org/10.1017/9781009325844.008>
- Feddes, R.A., Kowalik, P.J. and Zardny, H. 1978. *Simulation of Field Water Use and Crop Yield*. Wiley.
- Fourie, A.B., Rowe, D. and Blight, G.E. 1999. The effect of infiltration on the stability of the slopes of a dry ash dump. *Géotechnique*, **49**, 1–13, <https://doi.org/10.1680/geot.1999.49.1.1>
- Fowler, H.J., Lenderink, G. *et al.* 2021. Anthropogenic intensification of short-duration rainfall extremes. *Nature Reviews Earth & Environment*, **2**, 107–122, <https://doi.org/10.1038/s43017-020-00128-6>
- Gariano, S.L. and Guzzetti, F. 2016. Landslides in a changing climate. *Earth-Science Reviews*, **162**, 227–252, <https://doi.org/10.1016/j.earscirev.2016.08.011>
- Gavin, K. and Xue, J. 2008. A simple method to analyze infiltration into unsaturated soil slopes. *Computers and Geotechnics*, **35**, 223–230, <https://doi.org/10.1016/j.compgeo.2007.04.002>
- Geo-Slope International. 2020. *Heat and Mass Transfer Modelling with GeoStudio*. Geo-Slope International.
- Guo, B.W.L. 2021. *Reuse and sustainability of flood defences*. PhD thesis, Imperial College London.
- Harrison, A.M., Plim, J., Harrison, M., Jones, L.D. and Culshaw, M.G. 2012. The relationship between shrink–swell occurrence and climate in south-east England. *Proceedings of the Geologists' Association*, **123**, 556–575, <https://doi.org/10.1016/j.pgeola.2012.05.002>
- Hillel, D. 2004. *Introduction to Environmental Soil Physics*. Elsevier, Amsterdam.
- Huang, W., Loveridge, F., Briggs, K. and Smethurst, J. 2023. Forecast UKCP18 local projections climate change scenario data and resulting simulated pore water pressure data for clay earthworks. University of Leeds [Dataset], <https://doi.org/10.5518/1435>
- Hulme, M., Jenkins, G.J. *et al.* 2002. *Climate Change Scenarios for the United Kingdom: the UKCIP02 Scientific Report*. Centre for Climate Change Research, School of Environmental Sciences, University of East Anglia, Norwich.
- Indraratna, B., Fatahi, B. and Khabbazi, H. 2006. Numerical analysis of matric suction effects of tree roots. *Proceedings of the Institution of Civil Engineers – Geotechnical Engineering*, **159**, 77–90, <https://doi.org/10.1680/jgeeng.2006.159.2.77>

- Jenkins, G.J., Perry, M.C. and Prior, M.J. 2009. *The Climate of the UK and Recent Trends. UKCP09*. Met Office Hadley Centre, Exeter.
- Jones, P.D., Kilsby, C.G., Harpham, C., Glenis, V. and Burton, A. 2009. *UK Climate Projections Science Report: Projections of Future Daily Climate for the UK from the Weather Generator*. UK Climate Projections, Science Report.
- Lee, E.M. 2020. Statistical analysis of long-term trends in UK effective rainfall: implications for deep-seated landsliding. *Quarterly Journal of Engineering Geology and Hydrogeology*, **53**, 587–597, <https://doi.org/10.1144/qjehg2019-169>
- Lee, L.M., Gofar, N. and Rahardjo, H. 2009. A simple model for preliminary evaluation of rainfall-induced slope instability. *Engineering Geology*, **108**, 272–285, <https://doi.org/10.1016/j.enggeo.2009.06.011>
- Leung, A.K., Garg, A. and Ng, C.W.W. 2015. Effects of plant roots on soil-water retention and induced suction in a saprolite slope. *Engineering Geology*, **193**, 183–197, <https://doi.org/10.1016/j.enggeo.2015.04.017>
- Li, A.G., Yue, L.G., Tham, C. and Law, K.T. 2005. Field-monitored variations of soil moisture and matric suction in a saprolite slope. *Canadian Geotechnical Journal*, **42**, 13–26, <https://doi.org/10.1139/t04-069>
- Lieber, E., Demers, I., Pabst, T. and Bresson, É. 2022. Simulating the effect of climate change on performance of a monolayer cover combined with an elevated water table placed on acid-generating mine tailings. *Canadian Geotechnical Journal*, **59**, 558–568, <https://doi.org/10.1139/cgj-2020-0622>
- Loveridge, F.A., Spink, T.W., O'Brien, A.S., Briggs, K.M. and Butcher, D. 2010. The impact of climate and climate change on infrastructure slopes, with particular reference to southern England. *Quarterly Journal of Engineering Geology and Hydrogeology*, **43**, 461–472, <https://doi.org/10.1144/1470-9236/09-050>
- Lowe, J.A., Bernie, D. *et al.* 2018a. *UKCP18 Science Overview Report*. Met Office Hadley Centre, Exeter.
- Lowe, J.A., Murphy, J.M., Palmer, M.D. and Fung, F. 2018b. *UKCP18 Science Overview Report*. UK Climate Projections.
- LUL. 2019. *G0054B A4: Earth Structures – Guide for Slope Stability Analysis*. London Underground Ltd, London.
- Mair, R. 2021. *A review of earthworks management*, <https://www.networkrail.co.uk/who-we-are/our-approach-to-safety/stonehaven/> [accessed 18 October 2022].
- Meinshausen, M., Smith, S.J. *et al.* 2011. The RCP greenhouse gas concentrations and their extensions from 1765 to 2300. *Climatic Change*, **109**, 213–241, <https://doi.org/10.1007/s10584-011-0156-z>
- Min, S.K., Zhang, X., Zwiers, F.W. and Hegerl, G.C. 2011. Human contribution to more-intense precipitation extremes. *Nature*, **470**, 378–381, <https://doi.org/10.1038/nature09763>
- Moore, R., Carey, J.M. and McInnes, R.G. 2010. Landslide behaviour and climate change: predictable consequences for the Ventnor Undercliff, Isle of Wight. *Quarterly Journal of Engineering Geology and Hydrogeology*, **43**, 447–460, <https://doi.org/10.1144/1470-9236/08-086>
- Mualem, Y. 1976. A new model for predicting the hydraulic conductivity of unsaturated porous media. *Water Resources Research*, **12**, 513–522, <https://doi.org/10.1029/WR012i003p00513>
- Murphy, J.M., Harris, G.R. *et al.* 2018. *UKCP18 Land Projections: Science Report*. UK Climate Projections.
- O'Brien, A., Ellis, E.A. and Russell, D. 2004. Old railway embankment fill: laboratory experiments, numerical modelling and field behaviour. In: Jardine, R.J., Potts, D.M. and Higgins, K.G. (eds) *Advances in Geotechnical Engineering: Proceedings of the Skempton Memorial Conference, Hindhead, UK*. Thomas Telford, London, **2**, 911–921.
- Ozturk, U., Bozzolan, E., Holcombe, E.A., Shukla, R., Pianosi, F. and Wagener, T. 2022. How climate change and unplanned urban sprawl bring more landslides. *Nature*, **608**, 262–265, <https://doi.org/10.1038/d41586-022-02141-9>
- Palin, E.J., Stipanovic Oslakovic, I., Gavin, K. and Quinn, A. 2021. Implications of climate change for railway infrastructure. *Wiley Interdisciplinary Reviews: Climate Change*, **12**, e728, <https://doi.org/10.1002/wcc.728>
- Postill, H., Helm, P.R. *et al.* 2021. Forecasting the long-term deterioration of a cut slope in high-plasticity clay using a numerical model. *Engineering Geology*, **280**, 105912, <https://doi.org/10.1016/j.enggeo.2020.105912>
- Pk, S., Bashir, R. and Beddoe, R. 2021. Effect of climate change on earthen embankments in Southern Ontario, Canada. *Environmental Geotechnics*, **8**, 148–169, <https://doi.org/10.1680/jenge.18.00068>
- Rahimi, A., Rahardjo, H. and Leong, E.C. 2011. Effect of antecedent rainfall patterns on rainfall-induced slope failure. *Journal of Geotechnical and Geoenvironmental Engineering*, **137**, 483–491, [https://doi.org/10.1061/\(ASCE\)GT.1943-5606.0000451](https://doi.org/10.1061/(ASCE)GT.1943-5606.0000451)
- Robinson, E.L., Kay, A.L., Brown, M., Chapman, R., Bell, V.A. and Blyth, E.M. 2021. *Potential evapotranspiration derived from the UK Climate Projections 2018 Regional Climate Model ensemble 1980–2080 (Hydro-PE UKCP18 RCM)*. NERC EDS Environmental Information Data Centre, <https://doi.org/10.5285/eb5d9dc4-13bb-44c7-9bf8-c5980fcf52a4>
- Robinson, J.D., Vahedifard, F. and AghaKouchak, A. 2017. Rainfall-triggered slope instabilities under a changing climate: comparative study using historical and projected precipitation extremes. *Canadian Geotechnical Journal*, **54**, 117–127, <https://doi.org/10.1139/cgj-2015-0602>
- Rouainia, M., Davies, O., O'Brien, T. and Glendinning, S. 2009. Numerical modelling of climate effects on slope stability. *Proceedings of the Institution of Civil Engineers – Engineering Sustainability*, **162**, 81–89, <https://doi.org/10.1680/ensu.2009.162.2.81>
- Rouainia, M., Helm, P., Davies, O. and Glendinning, S. 2020. Deterioration of an infrastructure cutting subjected to climate change. *Acta Geotechnica*, **15**, 2997–3016, <https://doi.org/10.1007/s11440-020-00965-1>
- Sexton, D.M., McSweeney, C.F. *et al.* 2021. A perturbed parameter ensemble of HadGEM3-GC3.05 coupled model projections: part 1: selecting the parameter combinations. *Climate Dynamics*, **56**, 3395–3436, <https://doi.org/10.1007/s00382-021-05709-9>
- Smethurst, J.A., Clarke, D. and Powrie, W. 2006. Seasonal changes in pore water pressure in a grass covered cut slope in London Clay. *Géotechnique*, **56**, 523–537, <https://doi.org/10.1680/geot.2006.56.8.523>
- Smethurst, J.A., Clarke, D. and Powrie, W. 2012. Factors controlling the seasonal variation in soil water content and pore water pressures within a lightly vegetated clay slope. *Géotechnique*, **62**, 429–446, <https://doi.org/10.1680/geot.10.P.097>
- Smethurst, J.A., Briggs, K.M., Powrie, W., Ridley, A. and Butcher, D.J.E. 2015. Mechanical and hydrological impacts of tree removal on a clay fill railway embankment. *Géotechnique*, **65**, 869–882, <https://doi.org/10.1680/jgeot.14.P.010>
- Spink, T. 2020. Strategic geotechnical asset management. *Quarterly Journal of Engineering Geology and Hydrogeology*, **53**, 304–320, <https://doi.org/10.1144/qjehg2019-014>
- Tang, A.M., Hughes, P.N. *et al.* 2018. Atmosphere–vegetation–soil interactions in a climate change context; impact of changing conditions on engineered transport infrastructure slopes in Europe. *Quarterly Journal of Engineering Geology and Hydrogeology*, **51**, 156–168, <https://doi.org/10.1144/qjehg2017-103>
- Tarantino, A., Gallipoli, D. *et al.* 2016. Advances in the monitoring of geostucture subjected to climate loading. The 3rd European Conference on Unsaturated Soils, 12–14 September 2016, Paris, <https://doi.org/10.1051/e3sconf/20160904001>
- Tsiampousi, A., Zdravkovic, L. and Potts, D.M. 2017. Numerical study of the effect of soil–atmosphere interaction on the stability and serviceability of cut slopes in London clay. *Canadian Geotechnical Journal*, **54**, 405–418, <https://doi.org/10.1139/cgj-2016-0319>
- Vahedifard, F., Tehrani, F.S., Galavi, V., Ragno, E. and AghaKouchak, A. 2017. Resilience of MSE walls with marginal backfill under a changing climate: Quantitative assessment for extreme precipitation events. *Journal of Geotechnical and Geoenvironmental Engineering*, **143**, [https://doi.org/10.1061/\(ASCE\)GT.1943-5606.0001743](https://doi.org/10.1061/(ASCE)GT.1943-5606.0001743)
- Van Genuchten, M.T. 1980. A closed-form equation for predicting the hydraulic conductivity of unsaturated soils. *Soil Science Society of America Journal*, **44**, 892–898, <https://doi.org/10.2136/sssaj1980.03615995004400050002x>
- Vardon, P.J. 2015. Climatic influence on geotechnical infrastructure: a review. *Environmental Geotechnics*, **2**, 166–174, <https://doi.org/10.1680/envgeo.13.00055>
- Yamazaki, K., Sexton, D.M. *et al.* 2021. A perturbed parameter ensemble of HadGEM3-GC3.05 coupled model projections: part 2: global performance and future changes. *Climate Dynamics*, **56**, 3437–3471, <https://doi.org/10.1007/s00382-020-05608-5>
- Yu, Z., Eminue, O.O., Stirling, R., Davie, C. and Glendinning, S. 2021. Desiccation cracking at field scale on a vegetated infrastructure embankment. *Géotechnique Letters*, **11**, 88–95, <https://doi.org/10.1680/jgele.20.00108>
- Zhang, F., Wang, G., Kamai, T., Chen, W., Zhang, D. and Yang, J. 2013. Undrained shear behavior of loess saturated with different concentrations of sodium chloride solution. *Engineering Geology*, **155**, 69–79, <https://doi.org/10.1016/j.enggeo.2012.12.018>
- Zhang, F., Wang, G. and Peng, J. 2022. Initiation and mobility of recurring loess flowslides on the Heifangtai irrigated terrace in China: insights from hydrogeological conditions and liquefaction criteria. *Engineering Geology*, **302**, 106619, <https://doi.org/10.1016/j.enggeo.2022.106619>
- Zhang, L.L., Fredlund, D.G., Zhang, L.M. and Tang, W.H. 2004. Numerical study of soil conditions under which matric suction can be maintained. *Canadian Geotechnical Journal*, **41**, 569–582, <https://doi.org/10.1139/t04-006>